‘Pseudo’ Direct Drive Electrical machines with alternative winding configurations

Glynn Cooke, Kais Atallah

Department of Electronic and Electrical Engineering,
University of Sheffield
Sheffield, S1 4DE, U.K.

The integration of a magnetic gear and a brushless permanent magnet machine to realise a ‘pseudo’ direct drive (PDD®) with alternative winding configurations is investigated. It is shown topologies which facilitate the winding process and achieve a more robust stator construction exist. Comparisons with conventional PDD topologies which are essentially equipped with concentric windings have shown that similar efficiencies can be achieved, albeit at the expense of reduced torque densities. Furthermore, analysis of the magnetic forces exhibited by a pole-piece has shown that both the average and dynamic forces are significantly affected by the rated load condition, exacerbating the radial forces.

Index Terms— Magnetic gear, permanent magnet machines, manufacturing automation.

I. Introduction

As magnetically geared machines advance from technology demonstrators and prototypes, research is focusing on cost reductions and improved manufacturability. With the technology maturing and finding applications in a variety of fields from down-well oil and gas, automotive traction motors, aerospace actuators and marine propulsion the ease of manufacture and mechanical robustness are becoming key considerations, in addition to the electromagnetic performance.

The mechanical and magnetic integration of a magnetic gear and permanent magnet (PM) brushless machine gave rise to the so called ‘Pseudo’ Direct Drive (PDD®) [1]. As it develops toward volume manufacture for several applications many design decisions have already been considered. For example, in order to improve the mechanical integrity early prototypes are superseded by closed structures in which the high-speed rotor (HSR) is completely enclosed within the pole-piece rotor (PPR). This, however, makes position sensing for commutation purposes more challenging, requiring advanced control methods to be developed [2][3].

As can be seen in Fig. 1, concentric windings have been extensively employed in the design of PDDs, as this effectively decouples the selection of the number of poles on the stationary magnet array and the number of stator slots [1][4][5]. Therefore, this paper describes a method which significantly facilitates the realisation of the stationary permanent magnet array, while coupling the process of winding and pole-pair selections. This approach should facilitate the use of automated winding processes employed in low cost industrial induction machines, for example.

As can be seen in Fig. 3(a), in the proposed technique, a stationary permanent magnet pole is fixed on a stator tooth. This provides a significantly more robust fixing method and avoids the possibility of poles having to be mounted on the slot opening, Fig. 1. However, in addition to linking the selection of the number poles and the number of slots, in this topology, the magnetic fluxes produced by the stationary permanent magnet array, will also exhibit a significantly

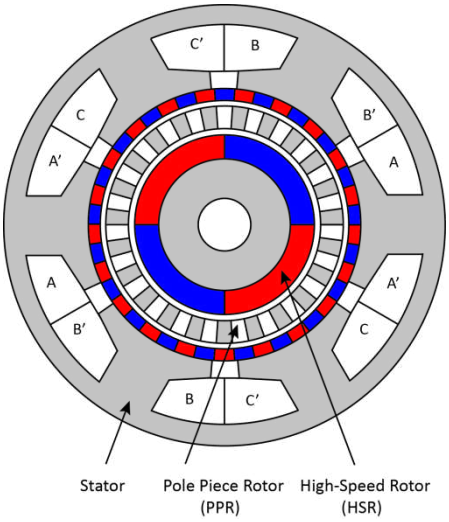

Fig. 1 Conventional concentric winding and stationary PM magnet array

stronger coupling with the windings as they return through the teeth and the back-iron.

It is shown that a significant advantage, in terms of ease of manufacture, can be achieved whilst maintaining torque densities in excess of 45kNm/m^3, under natural air cooling conditions. Furthermore, this is achieved at power factors in excess of 0.9 and with current densities below 2A$_{rms}$/mm^2.

II. Proposed ‘Pseudo’ Direct Drive Machine

A. Gear Ratio Selection

The principle of operation of the proposed machine topologies remain consistent with those outlined in [1]. For the PDD shown in Fig. 1, Fig. 2 shows the harmonic spectra of the flux density waveforms in the air gap adjacent to stator, due to the PMs on the HSR, with and without the pole-pieces. The introduction of the ferromagnetic pole-pieces results in asynchronous harmonics, the largest of which (21-pole pair) couples with the 21 pole-pair stator PMs to transmit torque to the PPR. Meanwhile, the 2-pole fundamental synchronous harmonic couples with the winding to produce electromagnetic torque. The stator winding links to the

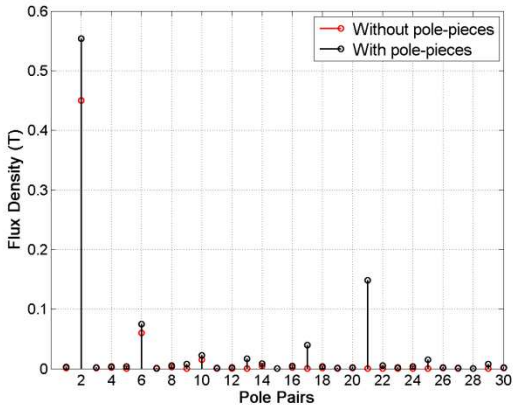

Fig. 2 Harmonic spectra of the flux density waveforms in the air gap adjacent to the stator due to the HSR PMs.

stationary PM array via an essentially constant flux, negligible EMF is induced as a result.

The realisation of the magnetic gear component should yield high airgap shear stress whilst maintaining low cogging torque. In turn the stator should strongly couple the fluxes from the HSR and those arising from the winding. Selecting a single tooth per stator magnet pole couples the pole number to the winding configuration and the number of stator teeth. Intrinsic to this is the selected number of electrical phases and in order to achieve a viable machine, the following conditions must be satisfied:

$$Q = nq \tag{1}$$

where $n = 1,2,3,\ldots$

$$p_l = \frac{Q}{k_{con}} \tag{2}$$

$$n_s = p_h + p_l \tag{3}$$

$$G_r = \frac{n_s}{p_h} \tag{4}$$

$$C_f = \frac{2 p_h n_s}{LCM(2 p_h, n_s)} = 1 \tag{5}$$

where q is the number of phases, Q is the number of stator slots, k_{con} is the number of consecutive stator magnets per pole, p_h and p_l are the number of pole pairs on the HSR and stationary magnet arrays, respectively, n_s is the number of modulating pole-pieces, G_r is the gear ratio and C_f is the Cogging Torque Factor [6].

Fig. 3(a) shows an example of a PDD, where each stator magnet pole is mounted on a stator tooth. However, the use of multiple teeth per stator pole is made possible by selecting the appropriate number of consecutive magnets of the same polarity ($k_{con} > 1$). This can result in a different winding configuration as shown in Fig. 3(b).

B. Winding Configurations

To analyse key electrical characteristics of the proposed machine configuration, parameters including winding factor are required. The winding configuration, where the armature pole pair number equals p_h, is determined using the method outlined in [7]. For no rotor or stator skewing the winding

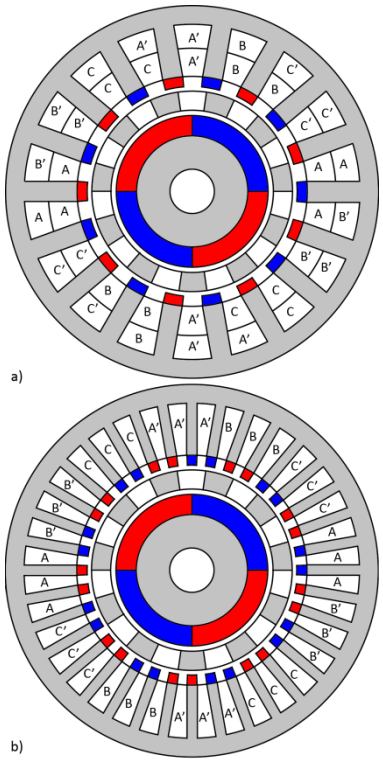

Fig. 3 Proposed realisation of PM magnet array and alternative winding with a) $k_{con} = 1$ and b) $k_{con} = 2$

factor for the fundamental component k_w is given by:

$$k_w = k_d \, k_p \tag{6}$$

Where, k_d is the distribution factor is given:

$$k_d = \frac{\sin(q_{ph} . \alpha_{ph} / 4)}{(q_{ph} / 2)\sin(\alpha_{ph} / 2)} \quad \text{for even } q_{ph} \tag{7}$$

$$k_d = \frac{\sin(q_{ph} . \alpha_{ph} / 4)}{q_{ph} \sin(\alpha_{ph} / 4)} \quad \text{for odd } q_{ph} \tag{8}$$

where,

$$\alpha_{ph} = \alpha_s t \tag{9}$$

$$q_{ph} = \frac{Q}{qt} \tag{10}$$

where α_s is the slot pitch and t is the greatest common divisor (GCD) of Q and p_h. The pitch factor k_p is given by:

$$k_p = \sin\left(\frac{\sigma_w}{2}\right) \tag{11}$$

where the coil span σ_w is given:

$$\sigma_w = \frac{2\pi \, p_h \, y_q}{Q} \tag{12}$$

where y_q is the number of whole slots per pole. An example of such a dual layer distributed winding, for the machine in Fig. 3(a), is shown in Fig. 4.

III. Simulation Studies

Finite element analysis enabled the determination of the key parameters, including the fundamental airgap flux density, transmitted torque and flux linkage, used to investigate various topologies. The parameters of machines under investigation are given in Table I. As it is the case for other machine

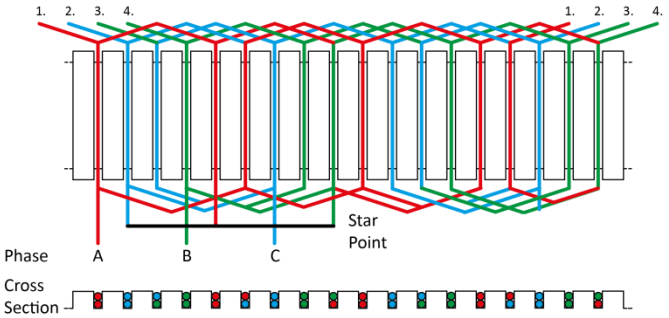

Fig. 4 Alternative winding for machine with $p_h = 2$, $n_S = 11$, $p_l = 9$

topologies, demagnetization can result from excessive armature currents, and this must be considered at the design stage. Albeit, PDDs exhibit relatively lower current loading, due the pull-out torque of the magnetic gear element, which imposes a maximum transmittable electromagnetic torque. Where applicable the quoted equivalent shear stress values are taken at the gear element pull-out torque.

TABLE I
PARAMETERS OF STUDIED ALTERNATIVE WINDING PDD'S

Quantity	Value
HSR Pole Pairs	2-8
Gear Ratio	4-15
Cogging Torque Factor	1
Stator Bore Diameter	126mm
Stator Outer Diameter	176mm
Number of Electrical Phases	3
Airgap length	1.5mm
Permanent Magnet (PM) Remanence	1.25T
Relative recoil permeability of PM	1.044

A single tooth per stationary magnet array pole ($k_{con} = 1$) accommodates the winding configuration but results in a reduction of the stator magnet volume, and α is defined as the ratio of slot opening to slot pitch. Common values for induction machines may vary between 0.25 and 0.6 [8]. For $\alpha = 0.5$, Fig. 5 shows the variation of the pull-out torque with gear ratio. It is can be seen that the transmitted torque is reduced compared to the conventional PDD, Fig. 1, employing a concentric winding. This is further illustrated in Figs. 6 and 7, which show the space harmonic spectra of the radial flux density waveforms in the airgap adjacent to the HSR. It can be seen that the magnitude of the asynchronous space harmonics, responsible for torque transmission, are reduced by adopting a 1-magnet pole per tooth configuration. However, this effect is alleviated for smaller values of α. Fig. 8 shows the variation of the equivalent shear stress with α, where it can be seen that it has a significant effect, but it can also be seen that shear stresses similar to those of the original machine can be achieved for smaller values of α.

Following the case of a single pole per tooth, consecutive magnets of the same orientation, $k_{con} = 2, 3, \ldots$ can be used to produce multiple teeth per stator magnet pole. This modification offers the machine designer more choice of gear ratios.

However, the resulting equivalent shear stresses, as shown

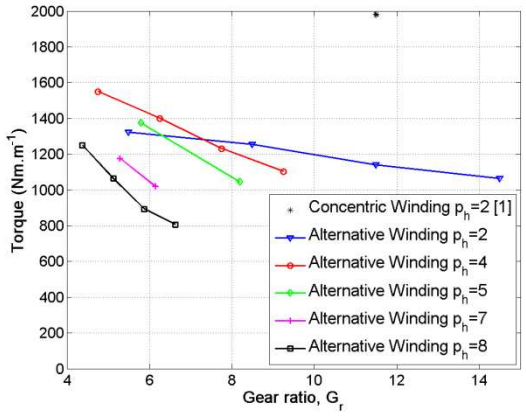

Fig. 5 Variation of normal operation torque with gear ratio and HSR pole number, p_h

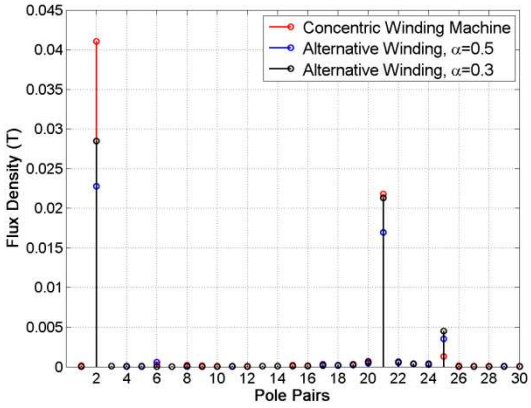

Fig. 6 Harmonic spectra of radial flux density resulting from the stationary magnet array, p_l=23 in the airgap adjacent to the HSR, p_h=2

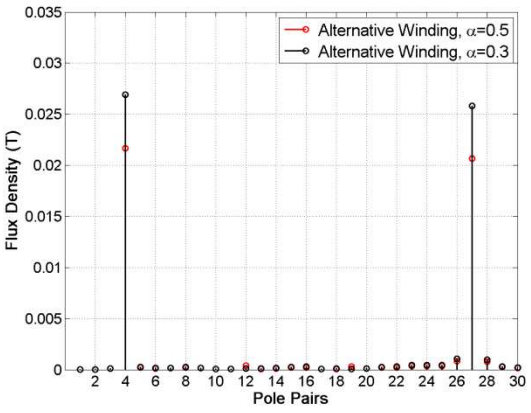

Fig. 7 Harmonic spectra of radial flux density resulting from the stationary magnet array, p_l=27 in the airgap adjacent to the HSR, p_h=4

in Fig. 9, are lower than those attained with a value of $k_{con} = 1$. Similarly to configurations with 1 stator pole per tooth, higher shear stresses are achieved with smaller values of α.

Fig. 10 and Fig. 11 show the variation of the required active length with α, in order to achieve the output torque of the machine equipped with concentric winding [1]. Fig. 12 and Fig. 13 shows the variation of efficiency at rated power, where only copper losses are considered. It can be seen that

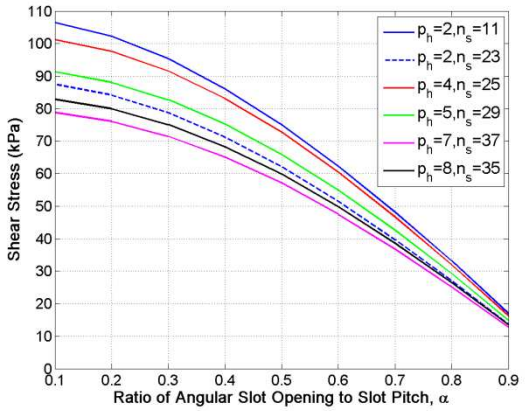

Fig. 8 Variation of shear stress at pull-out torque with the ratio of angular slot opening to slot pitch (Conventional concentric winding shear stress at pull-out torque, ~100kPa [1])

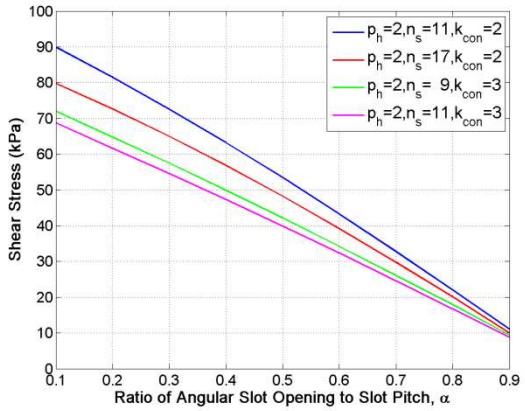

Fig. 9 Variation of shear stress at pull-out torque with the ratio of angular slot opening to slot pitch for $k_{con} > 1$ (Conventional concentric winding shear stress at pull-out torque, ~100kPa [1])

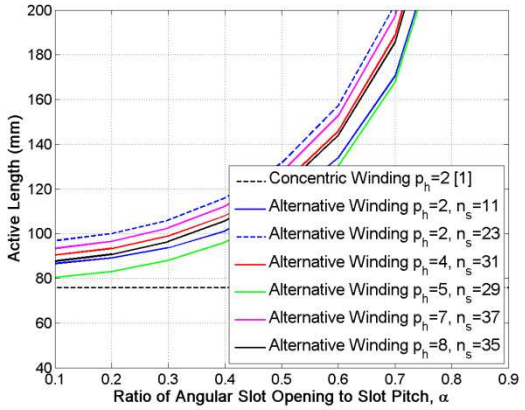

Fig. 10 Variation of Required active length with the ratio of angular slot opening to slot pitch when $k_{con} = 1$

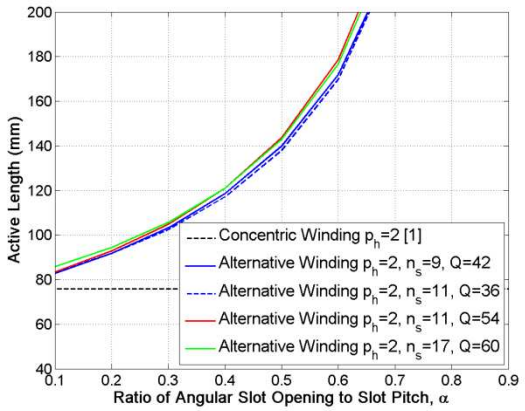

Fig. 11 Variation of Required active length with the ratio of angular slot opening to slot pitch when $k_{con} > 1$

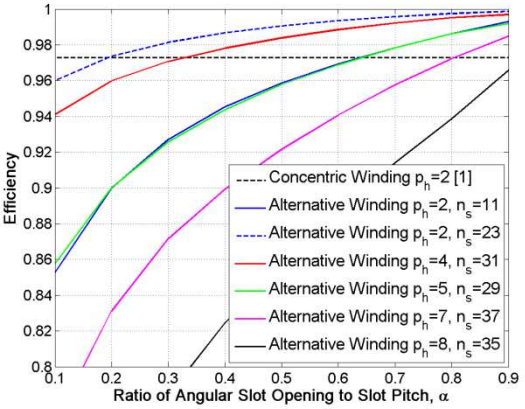

Fig. 12 Variation of Efficiency with the ratio of angular slot opening to slot pitch when $k_{con} = 1$ at rated power

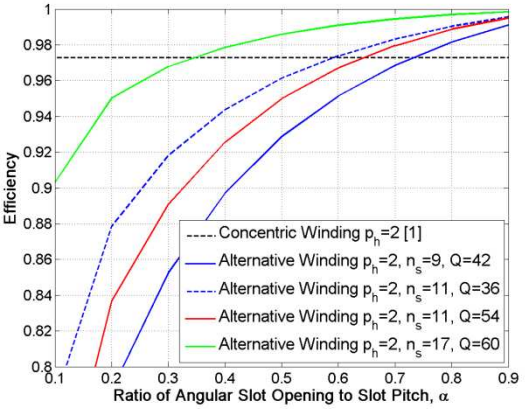

Fig. 13 Variation of Efficiency with the ratio of angular slot opening to slot pitch when $k_{con} > 1$ at rated power

efficiency increased with increased α , albeit at the expense of increased size. However, the PDDs with lower gear ratios can potentially be operated at higher speeds, as the mechanical constraints which restrict the maximum speed of the HSR are similar for all machines.

The resulting achievable power of those machines is shown in Fig. 14. The machines with lower gear ratios show increased efficiencies when operated at higher speed, as seen in Fig. 15 and Fig. 16, which show the variations of the efficiency with α .

In the proposed machine topology a single stator magnet is bonded to a single tooth. This leads to a stator tooth carrying the flux from a stator magnet, the magnets on the HSR and flux produced by the stator winding. This can lead to increased flux densities in the teeth and the back-iron. The resulting potential saturation can be alleviated by increasing the thickness of the back-iron and the teeth without increasing the

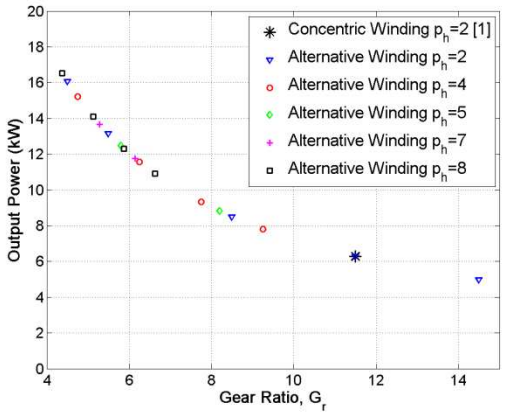

Fig. 14 Variation of potential output power with gear at the same HSR speed as in [1]

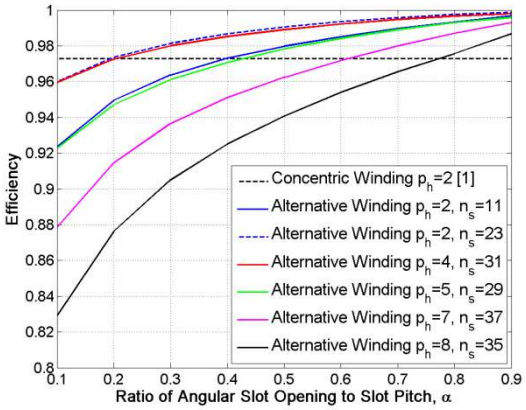

Fig. 15 Variation of Efficiency with the ratio of angular slot opening to slot pitch when k_{con} = 1 at the same HSR speed as in [1]

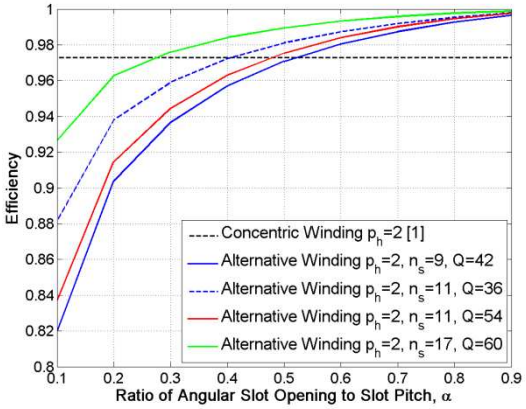

Fig. 16 Variation of Efficiency with the ratio of angular slot opening to slot pitch when k_{con} > 1 at the same HSR speed as in [1]

width of a stator permanent magnet. Although this may also reduce the iron losses, it may result in increased copper losses due to reductions in the slot areas.

Three designs have been selected for further analysis, including the iron losses, where the hysteresis P_{hyst}, classical eddy current P_{eddy} and excess eddy current P_{ex} components are considered and given by:

$$P_{iron} = P_{hyst} + P_{eddy} + P_{excess} \quad (14)$$

$$P_{hyst} = k_h B_m^{\beta} f \quad (15)$$

$$P_{eddy} = \frac{\sigma d^2}{12T}\int_0^T \left(\frac{dB(t)}{dt}\right)^2 .dt \quad (16)$$

$$P_{ex} = \frac{k_e}{T}\int_0^T \left(\frac{dB(t)}{dt}\right)^{1.5} .dt \quad (17)$$

where B_m is the peak magnetic flux density, f is the electrical frequency, d is the lamination thickness, σ is the electrical conductivity and k_h, β and k_e are constants determined from iron loss tests under sinusoidal flux density waveforms and covering a range of frequencies and flux densities. For the pole-pieces the frequency is different from that of the stator and is given by:

$$f_{PP} = \frac{G_r - 1}{G_r} f \quad (18)$$

Table II summarises the parameters and performance of the selected designs. It can be seen that PDD designs with alternative windings can be achieved with high equivalent airgap shear stresses as well as high efficiencies and power factors.

TABLE II
PARAMETERS OF OPTIMISED ALTERNATIVE WINDING PDDS

Quantity	**Machine A**	**Machine B**	**Machine C**
Winding Type	Concentric	Alternative	
HSR Pole Pairs	2	2	4
Gear Ratio	11.5	11.5	7.75
Number of slots	6	42	54
PPR speed (rpm)	500	500	500
Rated Torque (Nm)	120	120	120
Active diameter (mm)	178	178	178
Machine Axial Length (mm)	75	111	99
Copper losses (W)	175	102	165
Iron losses (W)	102	124	172
Efficiency	0.958	0.965	0.949
Power factor	0.95	0.99	0.98
Magnet Mass (kg)	3.27	4.46	3.74
Current Density ($A_{rms}mm^{-2}$)	1.5	1.3	1.7
Equivalent Airgap Shear Stress (kPa)	101.4	73.2	71.0

IV. FORCES ON THE POLE-PIECE ROTOR

In PDDs, the stator and HSR are very similar to those of conventional permanent magnet machines, and they would essentially exhibit similar stresses. However, the PPR is relatively unique, and its manufacture may pose some challenges, since the pole-pieces must be laminated and essentially held in a non-magnetic and non-conducting structure. Therefore, the understanding of the dynamic and static forces the pole-pieces are subjected to is essential for the successful realisation of the rotor.

At rated load, Fig. 17 and Fig. 18, show the variation of the radial and circumferential forces exhibited by a pole-piece over a 60 degree rotation of the PPR. These have been presented over 60 degrees for illustration purposes, since the

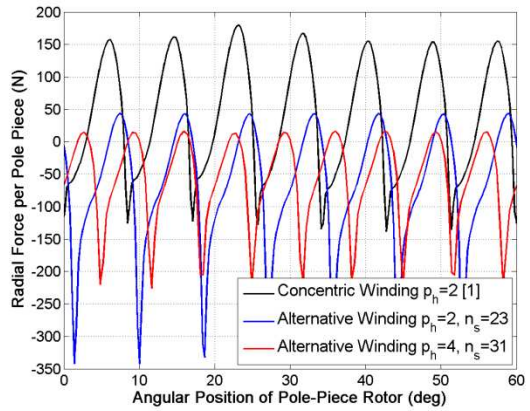

Fig. 17 Variation of the radial force (per pole piece) with PPR angular position at rated load

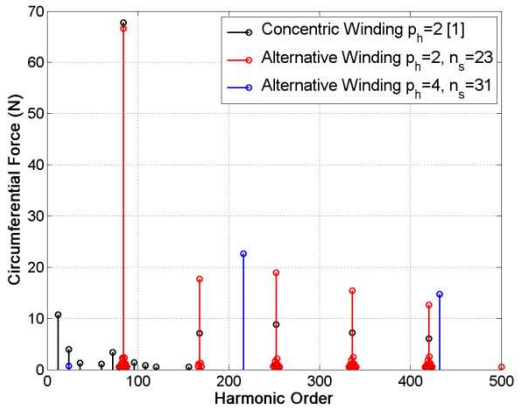

Fig. 20 Harmonic spectra of the circumferential force profile (per pole-piece) at rated load

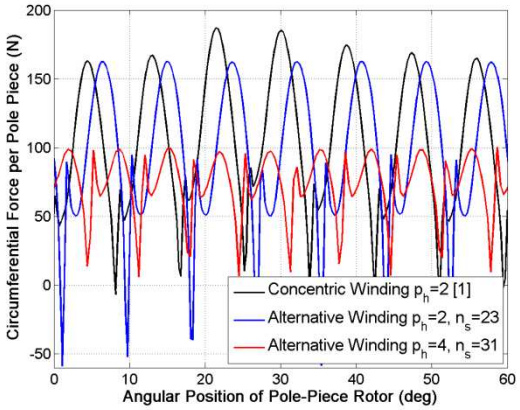

Fig. 18 Variation of the circumferential force (per pole piece) with PPR angular position at rated load

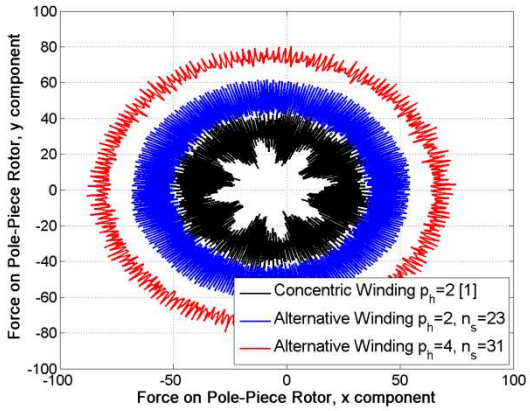

Fig. 21 Variation of total PPR forces at rated load

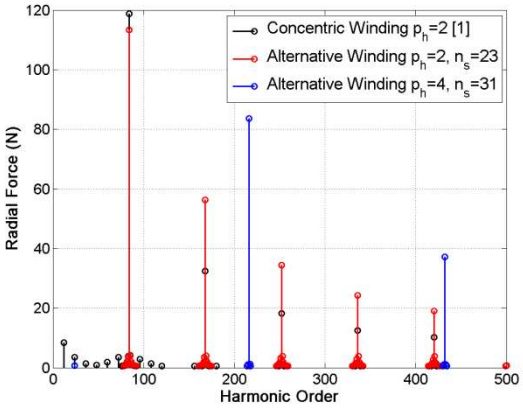

Fig. 19 Harmonic spectra of the radial force profile (per pole-piece) at rated load

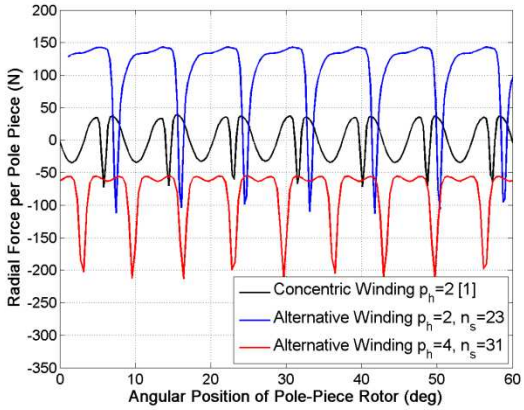

Fig. 22 Variation of the radial force (per pole piece) with PPR angular position at no load

period for the forces depends on the gear ratio. If the gear ratio is non-integer the period is p_h rotations of the PPR and n_s rotations of HSR. If the gear ratio is integer, the period is one rotation of the PPR and G_r rotations of the high-rotor. Therefore, for machines A and B, the period is 720º rotation of the PPR, while for machine C the period is 1440º rotation of the PPR. The average radial forces for machines are A, B and C are 36N, -70N and -59N, respectively.

Fig. 19 and Fig. 20, show the harmonic spectra of the radial and circumferential forces exhibited by a pole-piece. It can be seen that for the 3 machines the first largest harmonic order is $2\,p_h\,p_l$. The corresponding frequencies of the harmonics are given by:

$$\omega_n = \frac{n}{p_h}\omega_{pp} \tag{19}$$

where n is the harmonic order and ω_{pp} is the speed of the PPR. Fig. 21 shows the contour of the total force on the PPR

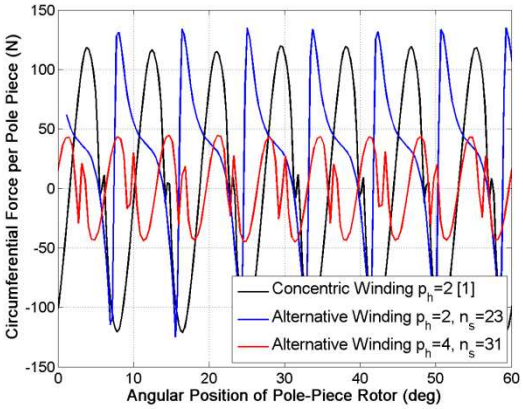

Fig. 23 Variation of the circumferential force (per pole piece) with PPR angular position at no load

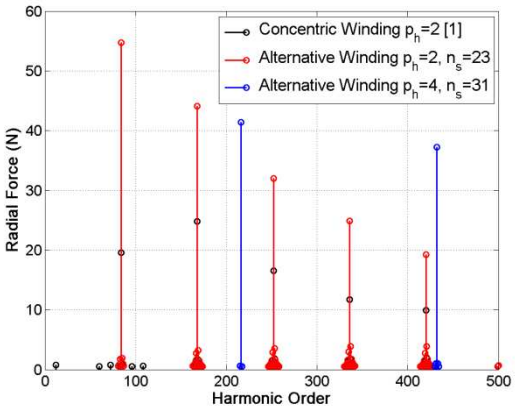

Fig. 24 Harmonic spectra of the radial force profile (per pole-piece) at no load

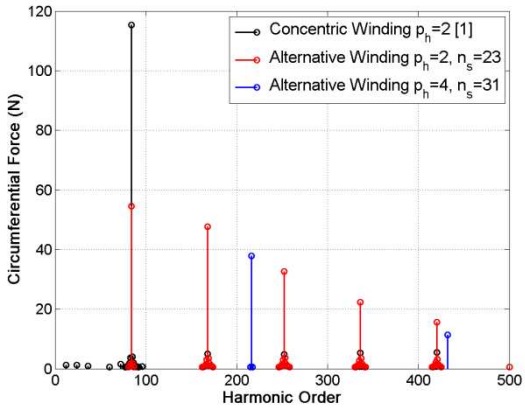

Fig. 25 Harmonic spectra of the circumferential force profile (per pole-piece) at no load

rotor over a 360° rotation of the PPR, where it can be seen that the PPR rotor equipped alternative windings exhibit larger unbalanced magnetic pull. At no load, Fig. 22 and Fig. 23, show the variation of the radial and circumferential forces exhibited by a pole-piece. The average radial force during the no-load condition for machines A, B and C are 0.5N, 107N and -82N, respectively. It can be seen that the average forces exhibited by a pole-piece are significantly affected by the load condition. Fig. 24 and Fig. 25, show the harmonic spectra of the radial and circumferential forces exhibited by a pole-piece. Fig. 26 shows the contour of the total force on the PPR over a

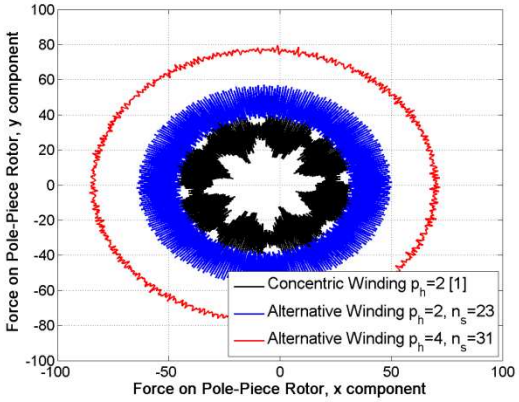

Fig. 26 Variation of total PPR forces at no load

360° rotation of the PPR. It can be seen that the average unbalanced magnetic pull is similar to the rated condition.

V. CONCLUSION

A technique for the selection of PDDs equipped alternative windings is presented. Simulation studies and comparisons with an existing PDD equipped concentric winding are undertaken. It is shown that PDDs with alternative windings can be realised, albeit with reduced torque density. Nevertheless, shear stresses and power factors in excess of 70kPa and 0.98, respectively, can still be achieved. Special attention was given to the forces exhibited by a pole-piece, and it was shown that both the average and dynamic forces are affected by the load condition.

ACKNOWLEDGMENT

This work was supported by the European Project INNWIND.EU and Magnomatics Ltd.

REFERENCES

[1] K. Atallah, J. Rens, S. Mezani, and D. Howe, "A Novel 'Pseudo ' Direct-Drive Brushless Permanent Magnet Machine," IEEE Trans. Magn., vol. 44, no. 11, pp. 4349–4352, 2008.

[2] M. Bouheraoua, J. Wang, and K. Atallah, "Observer Based State Feedback Controller Design for Pseudo Direct Drive using Genetic Algorithm," in 6th IET International Conference on Power Electronics, Machines and Drives (PEMD), 2012, pp. 1–6.

[3] M. Bouheraoua, J. Wang, and K. Atallah, "Speed control for a Pseudo Direct Drive permanent magnet machine with one position sensor on low-speed rotor," 2013 Int. Electr. Mach. Drives Conf., pp. 986–992, May 2013.

[4] S. Gerber and R. Wang, "Analysis of the End-Effects in Magnetic Gears and Magnetically Geared Machines," in International Conference on Electrical Machines (ICEM), 2014, pp. 396–402.

[5] D. J. Evans and Z. Q. Zhu, "Optimal torque matching of a magnetic gear within a permanent magnet machine," IEEE Int. Electr. Mach. Drives Conf., pp. 995–1000, 2011.

[6] Z. Q. Zhu and D. Howe, "Influence of design parameters on cogging torque in permanent magnet machines," IEEE Trans. Energy Convers., vol. 15, no. 4, pp. 407–412, 2000.

[7] N. Bianchi and M. Dai Pre, "Use of the star of slots in designing fractional-slot single-layer synchronous motors," IEE Proc. - Electr. Power Appl., vol. 153, no. 3, p. 459, 2006.

[8] E. K. Appiah, A. A. Jimoh, G. M'boungui, and J. L. Munda, "Effects of slot opening on the performance of a six phase squirrel cage induction machine using finite element and field analysis," in IEEE AFRICON Conference, 2013, pp. 0–4.